Effect of seed layer on the performance of ZnO nanorods-based photoanodes for dye-sensitized solar cells

Effect of seed layer on the performance of ZnO nanorods-based photoanodes for dye-sensitized solar cells

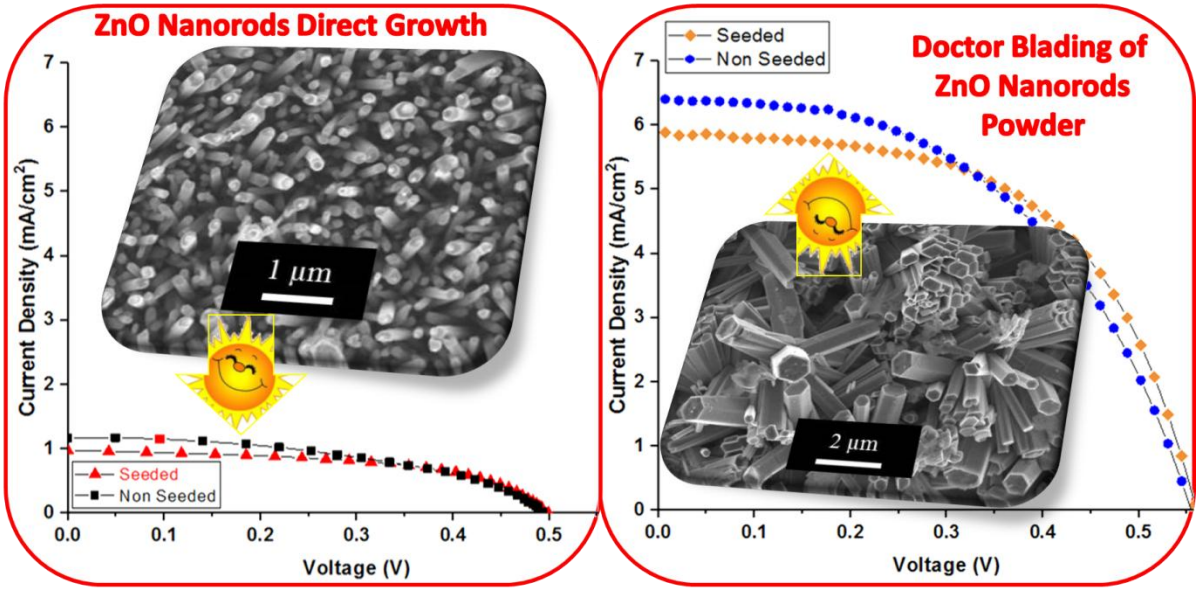

Highlights:

- Zinc oxide nanorods were synthesized by cheap and simple CBD method
- Pre-seeding of FTO glass substrates improve aspect ratio and alignment of nanorods
- Transmittance of the film can be enhanced by pre-seeding the FTO glass substrate
- Pre-seeding improves fill factor but lowers short-circuit current density of DSSC
- DSSC photovoltaic performance is affected by the pre-seeding deposition technique

Effect of seed layer on the performance of ZnO nanorods-based photoanodes for dye-sensitized solar cells

Nadia Shahzad[a], Zamarrud Shah[b], Muhammad Imran Shahzad[b], Kashan Ahmad[a], Diego Pugliese[c]

[a]*US-Pakistan Centre for Advanced Studies in Energy (USPCAS-E), National University of Science and Technology (NUST), 44000 Islamabad, Pakistan*

[b]*Nanosciences and Technology Department (NS&TD), National Centre for Physics (NCP), 44000 Islamabad, Pakistan*

[c]*Applied Science and Technology Department, Politecnico di Torino, Corso Duca degli Abruzzi 24, 10129 Torino, Italy*

[*] Corresponding author: e-mail: nadia-shahad@live.com, Tel. +92 313 6965143.

Abstract:

In this paper, zinc oxide nanorods (ZnO NRs) were synthesized by chemical bath deposition (CBD) method at 90 °C by using zinc nitrate hexahydrate and hexamethylenetetramine as precursors. In a first stage, the ZnO NRs were grown on un-seeded and pre-seeded fluorine-doped tin oxide (FTO) glass substrates by direct chemical bath deposition (CBD) method to study the effect of the ZnO seed layer on the NRs structural, morphological and optical properties. The X-Ray diffraction (XRD) analysis performed on the pre-seeded NRs revealed a pure ZnO hexagonal wurtzite crystalline phase, while the field emission scanning electron microscopy (FESEM) unveiled that the pre-seeded NRs exhibit a smaller diameter, higher density, higher aspect ratio and improved orientation along the c-axis with respect to the un-seeded NRs. In a second stage, the powder obtained by aging, centrifuging and drying the precipitates formed during the CBD growth was analyzed by XRD to assess its crystal structure and phase purity and subsequently coated on un-seeded and pre-seeded FTO glass substrates by doctor blade technique. The ZnO NRs-based seeded and non-seeded films fabricated by the two methods were finally used as photoanodes in dye-sensitized solar cells (DSSCs). Interestingly, the employment of pre-seeded ZnO NRs films deposited by doctor blade technique in comparison to the counterpart electrodes synthesized by direct CBD growth has led to a noticeable increase in the DSSC photoconversion efficiency from 0.35 to 1.86%. On the other hand inclusion of seed layer has effectively improved the fill factor of DSSC IV curves for both photoanode deposition techniques.

Keywords: ZnO, Nanorods, Chemical bath deposition, Doctor blade, Seed layer, Dye-sensitized solar cells

1. Introduction

In the last few decades, DSSCs have attracted a noticeable research interest due to their several attractive features such as low production cost, ease of fabrication and relatively high

conversion efficiency, which make them a sound alternative to the conventional silicon-based solar cells. In a DSSC, the photoanode plays two fundamental functions, namely it governs the collection and transportation of photo-excited electrons from the sensitizer to the external circuit and acts as a scaffold layer for dye adsorption [1]. Consequently, the photoanode should possess a high electron mobility and a high surface area for the dye loading [2]. The typical DSSC photoanode usually consists of wide band gap semiconducting metal oxides such as titanium dioxide (TiO_2) and zinc oxide (ZnO) deposited on transparent conducting oxide (TCO) substrates. The morphology and composition of the semiconductor oxides have a significant impact on the DSSC photovoltaic performance. Since the seminal paper published by Michael Grätzel and Brian O'Regan in 1991 [3], nanoparticles-based photoanodes have been extensively employed in DSSCs. Nanoparticles exhibit high surface area which enhances the dye loading efficiency, but their surfaces act as grain boundaries thus hindering the charge transfer and enhancing the recombination losses. In this scenario, the NRs geometry is highly desirable for application in DSSCs, as charge transfer occurs in continuous crystals.

ZnO, group II-VI semiconductor material, has been extensively explored due to its high band gap (3.37 eV), high exciton binding energy (60 meV), stability at high temperature and promising optical properties. Despite ZnO is not a novel material, nevertheless its ability to grow in different nanostructured morphologies with high surface area for dye loading, such as nanotowers, nanovolcanoes, nanorods, nanotubes and nanoflowers [4], has made the interest in it always renewed. ZnO nanostructures can be synthesized by different techniques exploiting both physical and chemical methods, such as vapour phase transport (VPT) [5], chemical vapour deposition (CVD) [6], pulsed laser deposition (PLD) [7], chemical bath deposition (CBD) [8, 9], hydrothermal deposition [10] and electrochemical deposition [11]. Among the different solution-phase synthesis processes, which are intrinsically cost effective, chemical bath deposition method is particularly advantageous as it does not require sophisticated instrumentation, high temperature, high pressure or vacuum. The whole deposition takes place in one bath and easy control over the bath parameters results in the various morphologies.

The nanostructures of ZnO have a wide range of applications encompassing different fields. Depending on the targeted application, nanostructures with various morphology and size have been explored. The one-dimensional (1-D) nanostructured morphologies such as the nanorods and the nanowires have greater potential due to their tuneable electronic and optoelectronic properties. These nanostructures have been extensively exploited in different applications, particularly in light emitting diodes (LEDs) [12], field effect transistors (FETs) [13], gas sensors [14], nanogenerators [15] and photovoltaic devices [16].

In recent years, the effect of different seed layers on the morphology, diameter and density of nanowires grown on them has been studied. Subsequently, DSSCs employing pre-seeded nanowires as the photoanode material have been fabricated and their electrical parameters have been measured. The impact of the seed layer doping on the DSSCs photovoltaic performance has also been evaluated, and an overall increase of the cell efficiency in presence of doped seed layers has been assessed. To cite some valuable examples, ZnO nanowires grown on aluminum-doped zinc oxide (AZO) and un-doped ZnO seed layers showed energy conversion efficiencies in DSSC of 0.15 and 0.08%, respectively, under AM

1.5 solar radiation [17]. The energy conversion efficiency of a DSSC with a gallium-doped ZnO (GZO) seed layer was significantly enhanced by 86.36% as compared to that without doping. Aligned ZnO nanotubes grown on a transparent ZnO seed layer spin coated onto the FTO allowed obtaining a three times enhanced conversion efficiency compared to that measured using a non-aligned (un-seeded) nanotubes-based photoanode [18]. In light of the above reported experimental results, both un-doped and doped ZnO seed layers deposited onto FTO-coated glass substrates prior to the growth of the ZnO nanowires revealed to be crucial for improving the photovoltaic performance of DSSCs.

In this work, ZnO nanorods were grown/deposited on un-seeded and ZnO pre-seeded FTO substrates by chemical bath deposition/doctor blade techniques. The effect of the ZnO seed layer on the morphological, structural and optical features of ZnO nanorods was reported. The ZnO NRs-based seeded and non-seeded films were applied as the photoanodes to fabricate DSSCs. The current density-voltage characteristics were finally measured to explore the effect of the ZnO seed layer on photoelectric properties of the DSSCs.

2. Material and Methods

2.1. Chemicals and Materials

Zinc acetate dihydrate [$Zn(CH_3COO)_2 \cdot 2H_2O$, ≥99.0%], zinc nitrate hexahydrate [$Zn(NO_3)_2 \cdot 6H_2O$, ≥99.0%], hexamethylenetetramine (HMTA) [$C_6H_{12}N_4$, ≥99.0%] and fluorine-doped tin oxide [F:SnO_2, 22 Ω/cm^2]-coated glasses were purchased from Sigma-Aldrich. N719 dye [Ruthenizer 535bis-TBA] and electrolyte [Iodolyte AN50] were purchased from Solaronix. All these chemicals were used as received without further purification. The solvents used in this experiment were absolute ethanol [CH_3CH_2O, 99.8%] and distilled water.

2.2. Substrates preparation

The FTO-coated glass substrates (size 1.7 cm × 1.7 cm) were cleaned using a standard procedure. In detail, 20 min sonication in ultrasonic bath was performed first in acetone and then in 2-propanol, each step followed by washing with distilled water. Finally, the substrates were dipped in piranha solution (H_2SO_4:H_2O_2=3:1) for 10 min and rinsed with excess distilled water.

For seeded growth, 0.011 M zinc acetate dihydrate solution was prepared in ethanol and mildly stirred for 30 min. The seed layer solution was spin coated on pre-cleaned FTO-covered glass substrates at 2000 rpm for 20 s, followed by a baking at 120 °C for 15 min. This process was repeated four times, and a final annealing at 350 °C for 30 min was carried out.

2.3. Synthesis of ZnO NRs and photoanodes preparation by direct CBD growth

In a typical synthesis process, 0.1 M solutions of zinc nitrate hexahydrate and HMTA in 50 ml distilled water were prepared separately and stirred for 40 min. HMTA solution was mixed dropwise with zinc nitrate hexahydrate at continuous stirring for 40 min. Two FTO-

coated glass substrates, i.e. unseeded and pre-seeded, were immersed in the solution using Teflon holders. The beaker, previously covered with an aluminum foil, was transferred to the oven and kept for 3 h at a fixed temperature of 90 °C. The samples were then taken out from the oven, rinsed with distilled water and dried at room temperature. The prepared samples were finally annealed at 350 °C for 30 min and subsequently employed as photoanode material in DSSCs.

Precipitates were also formed during the CBD growth. They were aged for 48 h at room temperature and washed 4 to 5 times to normalize their pH. The precipitates were finally centrifuged and dried at 70 °C for 3 h to obtain a powder. The latter was further employed as photoanode material in DSSCs.

2.4. Photoanodes preparation by doctor blade technique and DSSCs fabrication

Keeping solvent to powder weight ratio equal to 2, the powder was dispersed in a solvent mixture of ethanol, water and acetic acid (volume ratio 66:32:2) and sonicated in ultrasonic bath for 4 h. Subsequently, a 1 cm^2 circular shaped ZnO layer was deposited using doctor blade technique on pre-cleaned FTO-covered glass substrates. After the deposition, the samples were dried at ambient temperature for 30 min and then thermally treated at 350 °C for 30 min in oven. The final thickness of the ZnO films was about 8 μm, as measured by using a profilometer (P.10 KLA-Tencor Profiler). Photoanodes were then heated at 70 °C for 10 min, soaked in a 0.4 mM N719 dye solution in absolute ethanol at room temperature for 1 h and finally rinsed with absolute ethanol to remove the non-adsorbed dye molecules. Photoanode sensitization time was fixed at 1 h based on the data reported in literature. Specifically, W. Chang *et al.* sensitized ZnO photoelectrodes in dye solution for 2 h [19], while A. Sedghi *et al.* reached the best performance of ZnO-based DSSCs by using a sensitization time of only 30 min [20]. Three different DSSCs were fabricated for each FTO-coated glass substrate, i.e pre-seeded and un-seeded, and for each deposition technique, i.e. CBD and doctor blade. The average values of the main DSSCs photovoltaic parameters as extracted from the current-voltage (*I*-*V*) curves are reported in the Results and discussion Section.

The counter electrode fabrication [21] and DSSCs assembly [22] were performed following the recipes reported in previously published works. The sensitized ZnO electrode and platinum counter electrode were assembled in a sandwich type cell using O-ring polydimethylsiloxane (PDMS) interconnections and Polymethylmethacrylate (PMMA) clamps. For preparation of the O-ring PDMS interconnections and membrane, a PDMS pre-polymer and a curing agent (SYLGARD® 184, Dow Corning) were mixed in 10:1 weight ratio and subsequently degassing at room temperature for 1h. Then the mixture was poured into the respective moulds and was cured at 70 °C for 1h in a convection oven [23].

Electrical contacts were made using 45 μm-thick conductive copper foils, insulated from each other by a PDMS membrane. The electrolyte was filled through a syringe connected with the O-ring PDMS interconnections. The active photovoltaic area of the cells was 1.0 cm^2, while the photovoltaic measurements were performed with a 0.22 cm^2 rigid black mask.

2.5. Characterization Techniques

The morphology of the ZnO NRs grown directly on the FTO-covered glass substrates and in the form of precipitates was evaluated using a field emission scanning electron microscope (FESEM, Zeiss Supra 40). The crystal structure and phase purity of the samples were assessed by using a X-ray diffractometer (Bruker D8). The optical properties, specifically the transmittance and the diffuse reflectance spectroscopy (DRS) of the ZnO NRs films grown by CBD on un-seeded and pre-seeded FTO-covered glass substrates were measured using an ultraviolet-visible (UV-Vis) spectrophotometer (PerkinElmer, Lambda 950). The DSSCs photovoltaic parameters, namely the open-circuit voltage (V_{oc}), the short-circuit current density (J_{sc}), the Fill Factor (FF) and the photoconversion efficiency (η) were obtained through the *I-V* measurements. These latter were carried out using a source measure unit (Keithley 2400) and a solar simulator (Keithlink) under a power intensity of 750 W/m^2.

3. Results and discussion

Figs. 1(a) and (b) show the FESEM top-view images of the ZnO NRs grown on the un-seeded and pre-seeded FTO-coated glass substrates, respectively. It is evident from both the images that the NRs are perfectly hexagonal in structure with flat surfaces at their tips. The average thickness of both films, as evaluated through profilometric analysis, resulted to be equal to 2.7 µm.

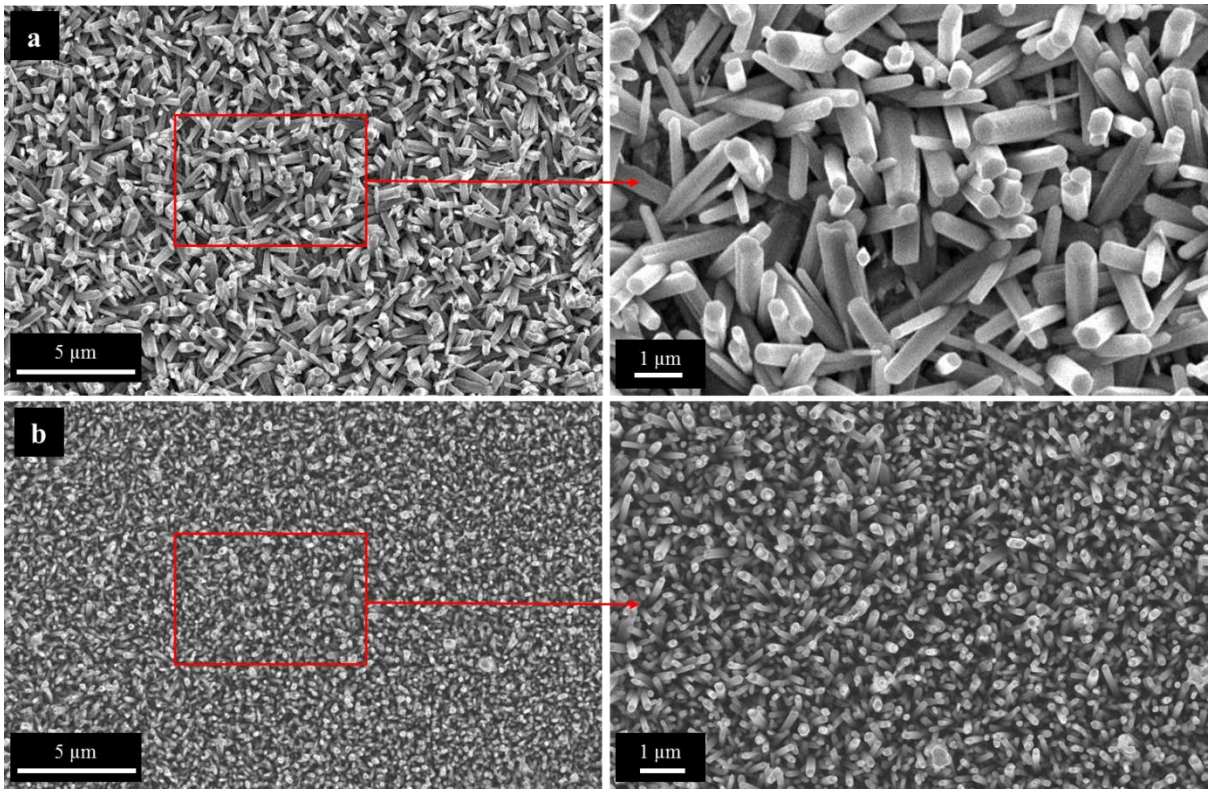

Fig. 1. FESEM top-view images at two different magnifications of ZnO NRs grown on **a)** un-seeded and **b)** pre-seeded FTO-covered glass substrates.

It is worthwhile noting that Figs. 1(a) and (b) are only a small selection of a large series of FESEM images taken for the determination of the most significant properties of the NRs grown on both the substrates. More in detail, the diameter, aspect ratio and statistical density reported here below are mean values evaluated on all the NRs observed in those images. As it can be clearly visualized from the enlarged image of Fig. 1a, the NRs grown in the absence of the seed layer show different diameter values in the range ~250-500 nm, with an average of 350 nm, an aspect ratio of 7.71, and a quite low statistical density equal to 1.26×10^6 nanorods per mm^2. In addition, few NRs with a larger diameter of ~650 nm and a smaller diameter of <200 nm were also observed but they were not considered for the aspect ratio calculation. The NRs display very random orientation with respect to the substrate surface. On the other hand, Fig. 1b shows that the employment of the seed layer prior to the NRs growth strongly influences the NRs growth parameters, as also derived from the previous literature [24]. The alignment was improved, while the seed layer of ZnO restricted the NRs diameters to well defined values in the range ~100-200 nm with an average of ~130 nm. The reduced diameter fluctuation is due to the limited spatial diameter variation exhibited by the ZnO seeds. This smaller diameter boosted the aspect ratio from 7.71 to 20.77 and, enough interestingly, led to an enhanced statistical density of 11.8×10^6 nanorods per mm^2, which is ~80% more than what measured for the unseeded growth. These results show that the ZnO NRs diameter, reproducibility and homogeneity over the substrate surface can be finely tuned through pre-seeding of the FTO-coated glasses.

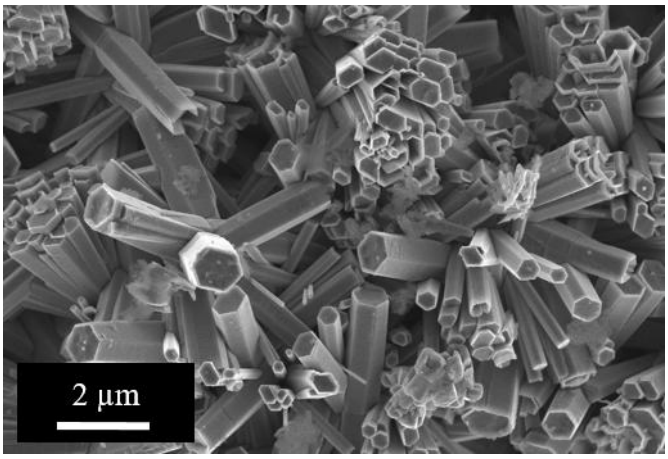

Fig. 2. FESEM image of the ZnO NRs powder obtained from the precipitates formed during the CBD growth.

The FESEM image of the powder collected from the chemical bath, as shown in Fig. 2, reveals a cluster structure with multi-branches NRs. It can be clearly assessed from the image that all the ZnO NRs originated from a single centre and are joined together through their wider base. The surface and lateral sides of the NRs are clean, smooth and display a hexagonal structure. Interestingly, the coalescence along the non-polar surfaces is also clear, and may be the consequence of the diameter expansion along these surfaces. The diameter and length of the NRs vary in the range 0.2-1 and 2-4 µm, respectively. The observed dissolution/etching of the NR tips, together with their structural modification towards a tube-like morphology, can be ascribed to the aging process, as precipitates were collected after 48

h. In another research work, Chae *et al.* attributed the change in the ZnO crystal morphology, from rod-like to tube-like, to the lowering of the growth temperature [25]. Actually, the metastable polar (0001) faces of the grown NRs can terminate with either Zn^{2+} or O^{2-} charges and are more reactive than other faces [26]. A selective dissolution of the metastable polar (0001) face of ZnO microrods in an aging time of two days, with consequent formation of a highly porous and non-polar hollow structure, was demonstrated by Vayssieres *et al.* [27]. Systems tend to reach thermodynamic colloidal stability due to aging conditions and therefore they may undergo some variations in size, morphology or structural properties [28]. At a lower temperature such as room temperature, the dissolution rate may be larger than the precipitation rate of the polar surface. Thus, the polar surface is more likely to be etched when aged.

The heterogeneous growth mechanism is well explained in a previously published work [29]. In addition to the heterogeneous growth, the homogeneous growth also takes place in the same bath. The crystal formation in a chemical bath can be divided into two steps, i.e. crystal nucleation and growth. Some of the nuclei formed in the solution adsorbed at the surface of the substrate. Subsequently, ZnO nuclei tended to aggregate to reduce their surface charge energies. Multi-NRs shared their single aggregate nuclei and formed clusters with multi-branches NRs.

Fig. 3 shows the XRD patterns of the ZnO NRs grown on un-seeded and pre-seeded FTO-coated glass substrates. The dominant diffraction peak is (002), which indicates that the NRs are oriented along the c-axis. During the growth process, the ZnO NRs tended to dominantly grow along the (002) crystal plane because of its lower surface free energy (1.6 J/m^2) as compared to the one of the planes (100) (3.4 J/m^2) and (101) (2.0 J/m^2) [17,30]. The diffraction peaks (002), (101) and (102) are exactly indexed to the hexagonal wurtzite ZnO phase (ICSD No. 01-079-0208) with lattice constants a = 3.2648 Å, b = 3.2648 Å and c = 5.2194 Å. No secondary phases were detected, thus proving a high purity of the grown NRs. The intensities of the diffraction peaks (002), (101), and (102) were found to increase as the seed layer was coated onto the FTO film prior to the NRs growth (Fig. 3). The increase in the intensity of the (002) peak proves the improved alignment of the NRs grown on the pre-seeded FTO-coated glass substrates, in agreement with the results of the FESEM analysis.

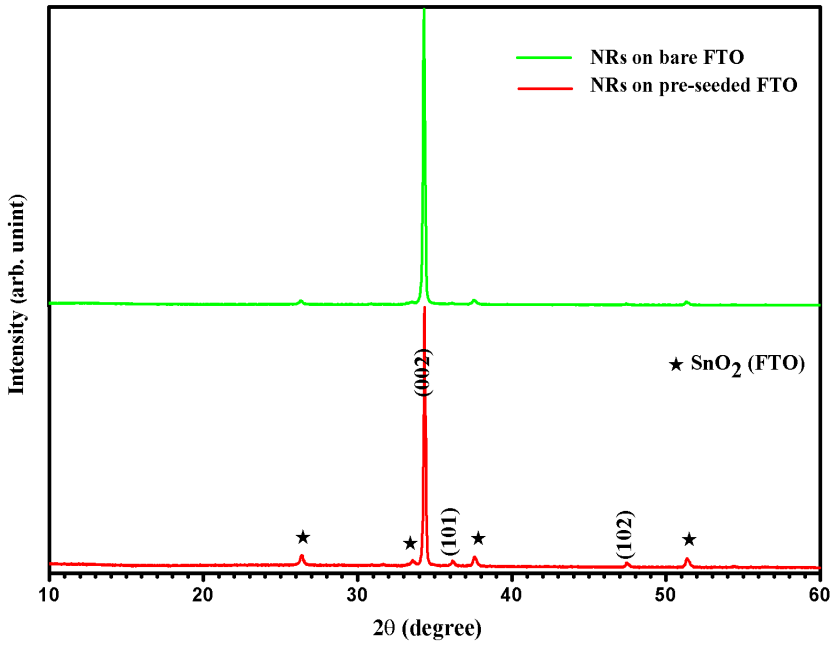

Fig. 3. XRD patterns of ZnO NRs grown on bare and pre-seeded FTO-coated glass substrates.

The XRD pattern of the ZnO powder collected from the chemical bath is depicted in Fig. 4. Throughout the angular range $20° \leq 2\theta \leq 80°$, all the peaks are in strong phase matching with the ZnO hexagonal wurtzite crystalline phase (ICSD No. 01-079-0208). The peaks observed at 2θ equal to 31.545°, 34.221°, 36.045°, 47.326°, 56.392°, 62.654°, 66.212°, 67.713°, 68.886°, 72.424° and 76.967° correspond to the reflection from the planes (001), (002), (101), (102), (110), (103), (200), (112), (201), (004) and (202), respectively. No other characteristic impurity peaks were observed, thus proving that even the residual powder collected at the bottom of the beaker at the end of the CBD growth was highly pure.

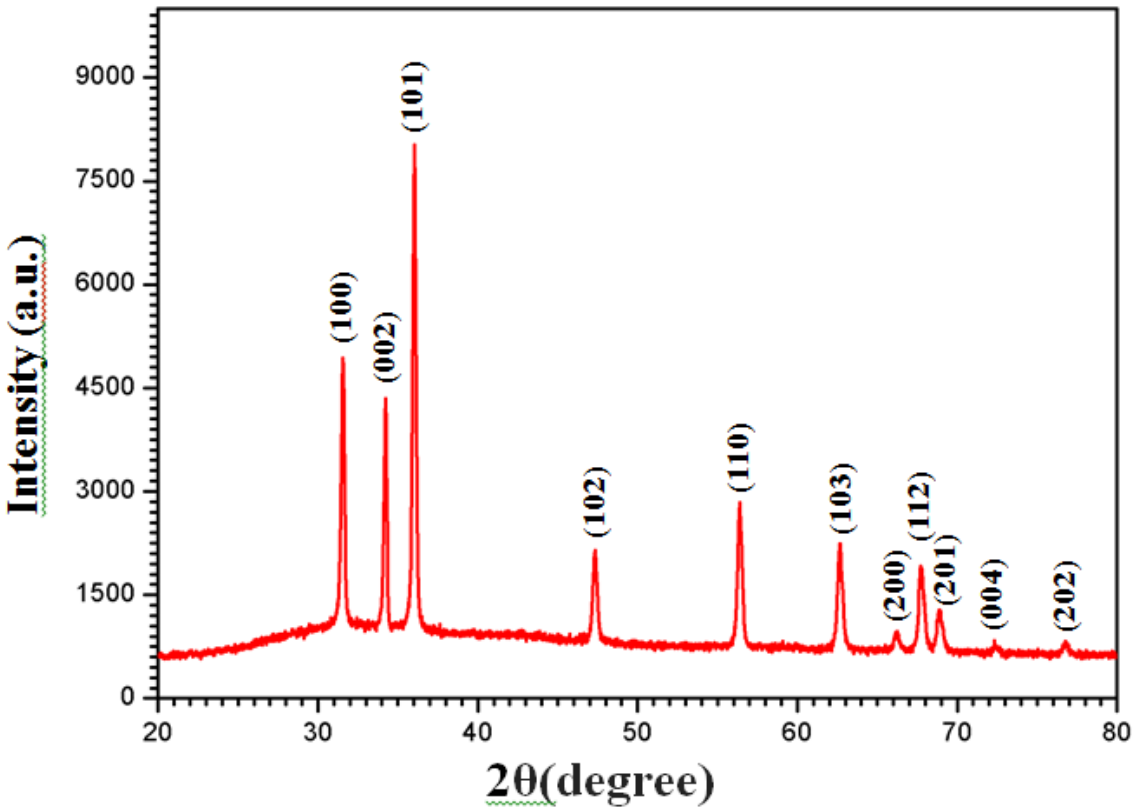

Fig. 4. XRD pattern of the ZnO powder collected from the chemical bath.

Fig. 5 illustrates that the pre-seeded and non-seeded films grown by direct method are transparent in the visible region and exhibit a high absorption edge in the UV region. Wang. *et al.* reported an increase in the transmittance of the ZnO nanorod arrays as a consequence of their enhanced vertical alignment and of the decrease in their diameter and length [31]. Therefore, the enhancement in transmittance of the ZnO NRs grown on pre-seeded FTO reported in this research work may be related to their improved vertical alignment and smaller diameter, which reduce the light scattering. Moreover, the lower overall transmittance in the visible region shown by our substrates with respect to the results reported by other researchers [18,32] for films grown by direct methods may be attributed to the higher film thickness (2.7 μm).

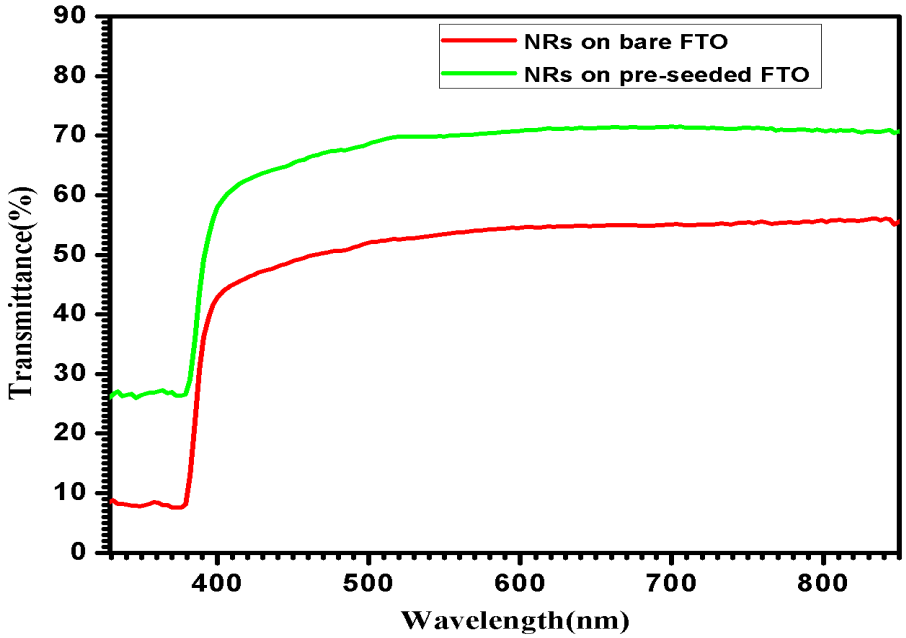

Fig. 5. Transmittance spectra of ZnO NRs grown on un-seeded and pre-seeded FTO-covered glass substrates.

To measure the optical band gap, the Diffuse Reflectance Spectroscopy (DRS) was performed on ZnO NRs grown on both bare and pre-seeded FTO-coated glass substrates. The Tauc plots were drawn using the Tauc relation (Eq. 1) and the Kubelka-Munk function (Eq. 2):

$$[F(R)h] = A\left(h - E_g\right)^n \qquad (1)$$

$$F(R) = \frac{(1-R)^2}{2R} \qquad (2)$$

where h is the Plank constant, v the incident light frequency, R the reflectance, E_g the band gap and n is 2 and 1/2 for direct and indirect band gap semiconductor materials [33], respectively. The plots reporting $[F(R)hv]^2$ on y-axis and hv on x-axis for both seeded and un-seeded ZnO NRs films are shown in Fig. 6. The band gap of the un-seeded ZnO NRs thin film was deduced from the plot to be 3.15 eV, while a value of 3.18 eV was obtained for the seed mediated growth. This slight increase in the band gap can be related to the reduced diameter of the ZnO NRs grown on pre-seeded FTO-covered glass substrates.

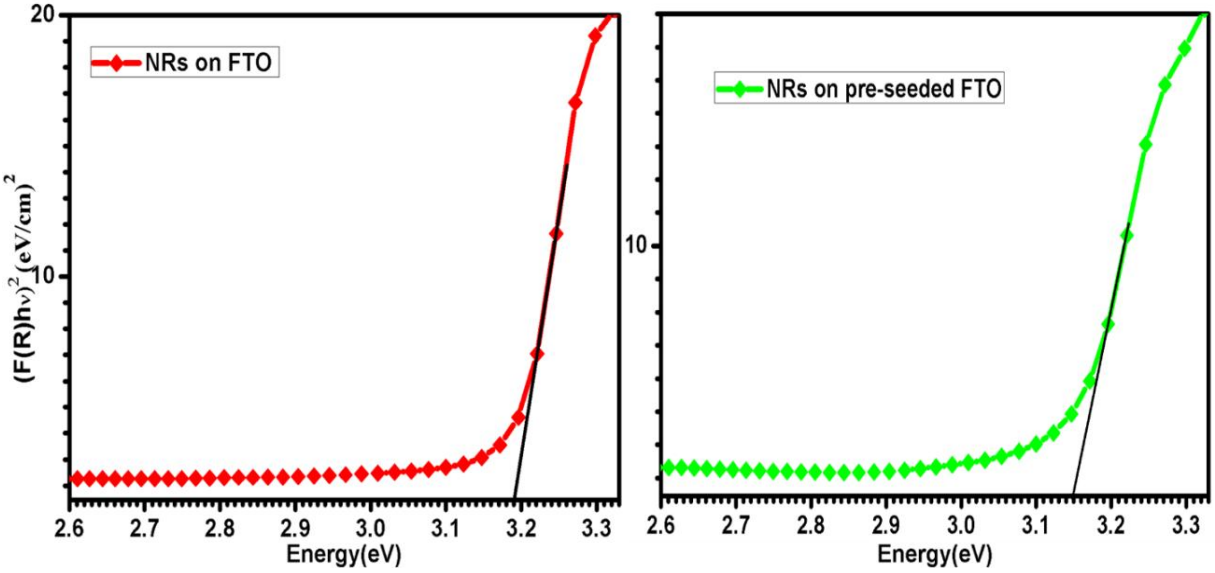

Fig. 6. Band gap evaluation from Tauc plots for ZnO NRs grown on both un-seeded and pre-seeded FTO-covered glass slices.

Fig. 7 shows the current density-voltage (*J-V*) characteristics of all the fabricated DSSCs. 1 h was selected as the most convenient soaking time of the photoanodes into the N719 sensitizer solution for avoiding the formation of Zn^{2+}/dye complexes and guaranteeing a high amount of absorbed dye molecules. The photovoltaic parameters obtained from the *I-V* measurements are summarized in Table 1.

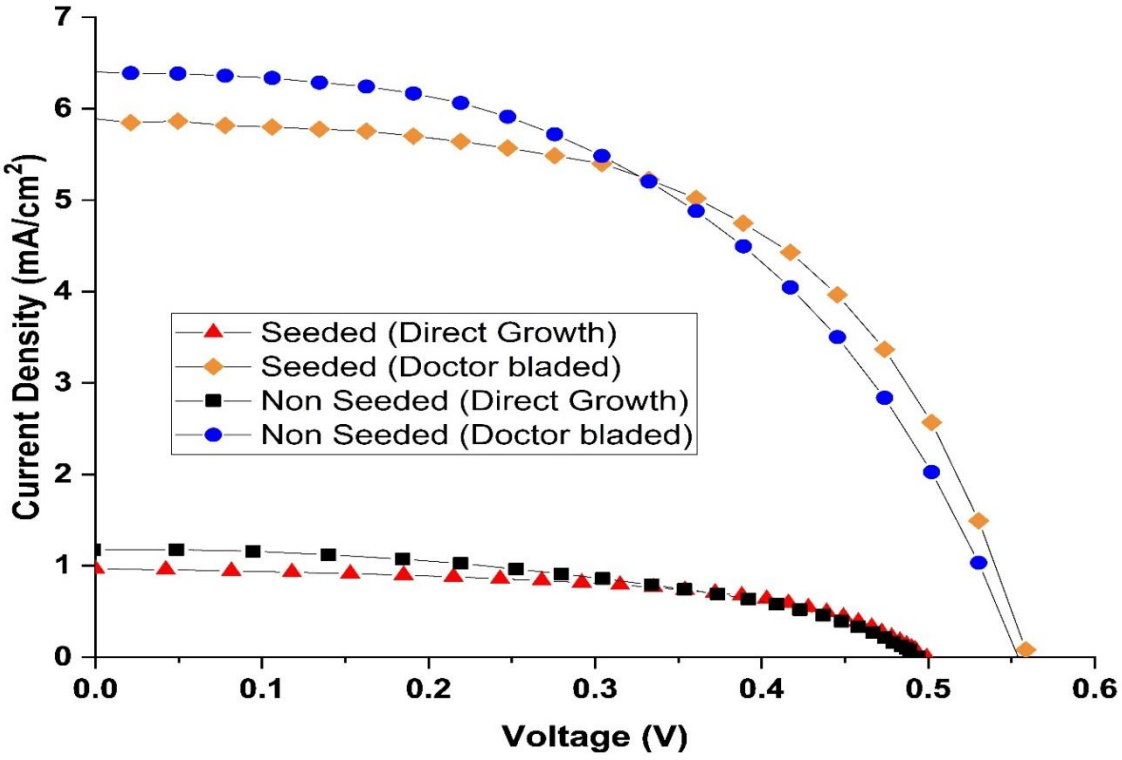

Fig. 7. *J-V* curves of the DSSCs based on un-seeded and pre-seeded ZnO NRs photoanodes fabricated by direct chemical bath deposition and doctor blade techniques.

Table 1 Photovoltaic parameters of all the manufactured DSSCs.

Technique: Chemical Bath Deposition

Photoanode	J_{sc} (mA/cm^2)	V_{oc} (V)	FF	η (%)
Un-seeded	1.18	0.49	0.46	0.35
Pre-Seeded	0.97	0.50	0.54	0.35

Technique: Doctor Blade

Photanode	J_{sc} (mA/cm^2)	V_{oc} (V)	FF	η (%)
Un-seeded	6.40	0.56	0.49	1.76
Pre-seeded	5.90	0.56	0.56	1.86

Independently of the photoanode fabrication method, the seed layer led to the increase of the DSSCs fill factor as a consequence of the decrease of their series resistance. For the direct growth technique, the low series resistance in the pre-seeded sample can be ascribed to the improved vertical alignment, small diameter and homogeneity of the NRs over the substrate surface. For the doctor blade technique, the ZnO seed layer was responsible for a better adhesion of the ZnO NRs to the FTO-coated glass substrate.

Interestingly, for both the deposition techniques, the J_{sc} values were observed to decrease when the photoanode film was grown/deposited on the seeded FTO, thus showing that the seed layer may result in a higher electron-hole recombination.

It is worthwhile noting that the open-circuit voltage value is higher in case of the photoanode deposited by doctor blade technique, possibly due to an increased homogeneity of the film and thus to a better dye coverage of the nanostructured oxide surface, and was unaffected by the presence of the seed layer for both the deposition techniques. The former assumption of the dependence of the open-circuit voltage on the dye loading behaviour is based on the literature evidences; in fact several researchers have reported that even a little variation in dye loading mechanism can be responsible for the variation of the electrical parameters of DSSCs such as V_{oc} for ZnO [34] as well as TiO_2 electrodes [35]. The latter experimental evidence, instead, is fully consistent with the fact that the V_{oc} depends only on the potential difference between the Fermi band edge and the redox couple potential (Iodolyte in our case) [36], while it is independent of the series resistance since the current flow is zero while measuring it.

4. Conclusions

ZnO NRs were successfully deposited on un-seeded and pre-seeded FTO-coated glass substrates by chemical bath deposition growth and by doctor blade technique. The morphology, structure, band gap and transparency of the NRs grown by CBD method on both

the un-seeded and pre-seeded substrates were thoroughly investigated and compared by using FESEM, XRD and UV/Vis spectroscopy. Results showed that, in addition to the smaller and controlled diameter, the density and alignment of the ZnO NRs along the c-axis were also improved by depositing the ZnO seed layer onto the FTO-covered glass substrates. This was confirmed by the FESEM images. The structural analysis by XRD revealed that the ZnO nanorod arrays grown on un-seeded and pre-seeded substrates are single crystalline in nature and were grown along the c-axis direction. The UV-Vis spectroscopy showed an improved transmittance of the pre-seeded film, which may be attributed to the smaller diameter of the rods and to an improved vertical orientation of the growth. The FESEM image of the powder collected from the chemical bath unveiled a cluster structure with multi-branches NRs, and each rod turned to tube-like morphology at its top due to the aging of the precipitates. This may be attributed to the dissolution of the c-axis polar surface (0001) due to its low chemical stability. The structural analysis of the powder collected from the bath is in good phase agreement with the ZnO hexagonal wurtzite phase. Finally, these ZnO NRs-based seeded and non-seeded films were employed as photoanode material to fabricate DSSCs. The electrical *I-V* measurements showed that the seed layer has led to the improvement of the fill factor and to the decrease of the short-circuit current density for both the deposition techniques. A maximum photoconversion efficiency of 1.86% was achieved by depositing the ZnO NRs on pre-seeded FTO-covered glass substrates using the doctor blade technique and by soaking the so-obtained photoanode in the Ru-based dye solution for 1 h.

Acknowledgment: The authors would like to thank Higher Education Commission, Pakistan for the financial support to conduct this research work.

5. References

[1] M.-E. Yeoh, K.-Y. Chan, 2017 Recent advances in photoanode for dyesensitized solar cells: a review, *Int. J. Energy Res.* **41** 2446–2467.

[2] K.S. Kim, H. Song, S.H. Nam, S.-M. Kim, H. Jeong, W.B. Kim, G.Y. Jung, 2012 Fabrication of an efficient light scattering functionalized photoanode using periodically aligned ZnO hemisphere crystal for dye sensitized solar cells, *Adv. Mater.* **24** 792–798.

[3] B. O'Regan, M. Grätzel, 1991 High-efficiency solar cell based on dye-sensitized colloidal TiO_2 films, *Nature* **353** 737–740.

[4] Y. Tong, Y. Liu, L. Dong, D. Zhao, J. Zhang, Y. Lu, D. Shen, X. Fan, 2006 Growth of ZnO nanostructures with different morphologies by using hydrothermal technique, *J. Phys. Chem. B* **110** 20263–20267.

[5] Y.X. Chen, M. Lewis, W.L. Zhou, 2005 Zno nanostructures fabricated through a double-tube vapor-phase transport synthesis, *J. Cryst. Growth* **282** 85–93.

[6] A. Umar, S. Lee, Y.H. Im, Y.B. Hahn, 2005 Flower-shaped ZnO nanostructures obtained by cyclic feeding chemical vapour deposition: structural and optical properties, *Nanotechnology* **16** 2462–2468.

[7] S. Choopun, H. Tabata, T. Kawai, 2005 Self-assembly ZnO nanorods by pulsed laser deposition under argon atmosphere, *J. Cryst. Growth* **274** 167–172.

[8] B. Cao, W. Cai, Y. Li, F. Sun, L. Zhang, 2005 Ultraviolet-light-emitting ZnO nanosheets prepared by a chemical bath deposition method, *Nanotechnology* **16** 1734–1738.

[9] Q. Li, J. Bian, J. Sun, J. Wang, Y. Luo, K. Sun, D. Yu, 2010 Controllable growth of well-aligned ZnO nanorod arrays by low-temperature wet chemical bath deposition method, *Appl. Surf. Sci.* **256** 1698–1702.

[10] B. Cheng, E.T. Samulski, 2004 Hydrothermal synthesis of one-dimensional ZnO nanostructures with different aspect ratios, *Chem. Commun.* **0** 986–987.

[11] L. Xu, Y. Guo, Q. Liao, J. Zhang, D. Xu, 2005 Morphological control of ZnO nanostructures by electrodeposition, *J. Phys. Chem. B* **109** 13519–13522.

[12] S.J. An, J.H. Chae, G.-C. Yi, G.H. Park, 2008 Enhanced light output of GaN-based light-emitting diodes with ZnO nanorod arrays, *Appl. Phys. Lett.* **92** 121108.

[13] B. Sun, H. Sirringhaus, 2005 Solution-processed zinc oxide field-effect transistors based on self-assembly of colloidal nanorods, *Nano Lett.* **5** 2408–2413.

[14] C. Wang, X. Chu, M. Wu, 2006 Detection of H_2S down to ppb levels at room temperature using sensors based on ZnO nanorods, *Sens. Actuators, B* **113** 320–323.

[15] Z.L. Wang, J. Song, 2006 Piezoelectric nanogenerators based on zinc oxide nanowire arrays, *Science* **312** 242–246.

[16] J.B. Baxter, A.M. Walker, K. van Ommering, E.S. Aydil, 2006 Synthesis and characterization of ZnO nanowires and their integration into dye-sensitized solar cells, *Nanotechnology* **17** S304–S312.

[17] J. Lv, J. Zhu, K. Huang, F. Meng, X. Song, Z. Sun, 2011 Tunable surface wettability of ZnO nanorods prepared by two-step method, *Appl. Surf. Sci.* **257** 7534–7538.

[18] M.-C. Kao, H.-Z. Chen, S.-L. Young, C.-C. Lin, C.-Y. Kung, 2012 Structure and photovoltaic properties of ZnO nanowire for dye-sensitized solar cells, *Nanoscale Res. Lett.* **7** 260.

[19] W.-C. Chang, C.-H. Lee, W.-C. Yu, C.-M. Lin, 2012 Optimization of dye adsorption time and film thickness for efficient ZnO dye-sensitized solar cells with high at-rest stability, *Nanoscale Res. Lett.* **7** 688.

[20] C. Bauer, G. Boschloo, E. Mukhtar, A. Hagfeldt, 2001 Electron injection and recombination in $Ru(dcbpy)_2(NCS)_2$ sensitized nanostructured ZnO, *J. Phys. Chem. B* **105** 5585–5588.

[21] N. Shahzad, D. Pugliese, M.I. Shahzad, E. Tresso, 2015 In-situ spectroscopic analyses of the dye uptake on ZnO and TiO_2 photoanodes for dye-sensitized solar cells, *J. Nanosci. Nanotechnol.* **15** 5993–6000.

[22] A. Sacco, A. Lamberti, D. Pugliese, A. Chiodoni, N. Shahzad, S. Bianco, M. Quaglio, R. Gazia, E. Tresso, C.F. Pirri, 2012 Microfluidic housing system: a useful tool for the analysis of dye-sensitized solar cell components, *Appl. Phys. A* **109** 377–383.

[23] A. Lamberti, A. Sacco, S. Bianco, E. Giuri, M. Quaglio, A. Chiodoni, E. Tresso, 2011 Microfluidic sealing and housing system for innovative dye-sensitized solar cell architecture, *Microelectron. Eng.* **88** 2308–2310.

[24] S.-H. Yi, S.-K. Choi, J.-M. Jang, J.-A. Kim, W.-G. Jung, 2007 Low-temperature growth of ZnO nanorods by chemical bath deposition, *J. Colloid Interface Sci.* **313** 705–710.

[25] K.-W. Chae, Q. Zhang, J.S. Kim, Y.-H. Jeong, G. Cao, 2010 Low-temperature solution growth of ZnO nanotube arrays, *Beilstein J. Nanotechnol.* **1** 128–134.

[26] A. Fulati, S.M. Usman Ali, M. Riaz, G. Amin, O. Nur, M. Willander, 2009 Miniaturized pH sensors based on zinc oxide nanotubes/nanorods, *Sensors* **9** 8911–8923.

[27] L. Vayssieres, K. Keis, A. Hagfeldt, S.-E. Lindquist, 2011 Three-dimensional array of highly oriented crystalline ZnO microtubes, *Chem. Mater.* **13** 4395-4398.

[28] L. Vayssieres, 2003 Growth of arrayed nanorods and nanowires of ZnO from aqueous solutions, *Adv. Mater*. **15** 464-466.

[29] Q. Ahsanulhaq, A. Umar, Y.B. Hahn, 2007 Growth of aligned ZnO nanorods and nanopencils on ZnO/Si in aqueous solution: growth mechanism and structural and optical properties, *Nanotechnology* **18** 115603.

[30] S. Liang, X. Bi, 2008 Structure, conductivity, and transparency of Ga-doped ZnO thin films arising from thickness contributions, *J. Appl. Phys.* **104** 113533.

[31] Z. Wang, B. Huang, X. Qin, X. Zhang, P. Wang, J. Wei, J. Zhan, X. Jing, H. Liu, Z. Xu, H. Cheng, X. Wang, Z. Zheng, 2009 Growth of high transmittance vertical aligned ZnO nanorod arrays with polyvinyl alcohol by hydrothermal method, *Mater. Lett.* **63** 130–132.

[32] R. Haarindraprasad, U. Hashim, S.C.B. Gopinath, M. Kashif, P. Veeradasan, S.R. Balakrishnan, K.L. Foo, P. Poopalan, 2015 Low temperature annealed zinc oxide nanostructured thin film-based transducers: characterization for sensing applications, PLoS One **10** e0132755.

[33] B.D. Viezbicke, S. Patel, B.E. Davis, D.P. Birnie, 2015 Evaluation of the Tauc method for optical absorption edge determination: ZnO thin films as a model system, *Phys. Status Solidi B* **252** 1700–1710.

[34] S.B. Ambade, R.S. Mane, A.V. Ghule, M.G. Takwale, A. Abhyankar, B. Cho, S.-H. Han, 2009 Contact angle measurement: A preliminary diagnostic method for evaluating the performance of ZnO platelet-based dye-sensitized solar cells, *Scr. Mater.* **61** 12–15.

[35] E. Dell'Orto, L. Raimondo, A. Sassella, A. Abbotto, 2012 Dye-sensitized solar cells: spectroscopic evaluation of dye loading on TiO_2. *J. Mater. Chem.* **22** 11364–11369.

[36] J. Chang, R. Ahmed, H. Wang, H. Liu, R. Li, P. Wang, E.R. Waclawik, 2013 ZnO nanocones with high-index {101} facets for enhanced energy conversion efficiency of dye-sensitized solar cells, *J. Phys. Chem. C* **117** 13836–13844.